Measurement of the masses and widths of the bottom baryons $\Sigma_b^{\pm}$ and $\Sigma_b^{*\pm}$

T. Aaltonen,[21] B. Álvarez González[z],[9] S. Amerio,[40] D. Amidei,[32] A. Anastassov[x],[15] A. Annovi,[17] J. Antos,[12] G. Apollinari,[15] J.A. Appel,[15] T. Arisawa,[54] A. Artikov,[13] J. Asaadi,[49] W. Ashmanskas,[15] B. Auerbach,[57] A. Aurisano,[49] F. Azfar,[39] W. Badgett,[15] T. Bae,[25] A. Barbaro-Galtieri,[26] V.E. Barnes,[44] B.A. Barnett,[23] P. Barria[hh],[42] P. Bartos,[12] M. Bauce[ff],[40] F. Bedeschi,[42] S. Behari,[23] G. Bellettini[gg],[42] J. Bellinger,[56] D. Benjamin,[14] A. Beretvas,[15] A. Bhatti,[46] D. Bisello[ff],[40] I. Bizjak,[28] K.R. Bland,[5] B. Blumenfeld,[23] A. Bocci,[14] A. Bodek,[45] D. Bortoletto,[44] J. Boudreau,[43] A. Boveia,[11] L. Brigliadori[ee],[6] C. Bromberg,[33] E. Brucken,[21] J. Budagov,[13] H.S. Budd,[45] K. Burkett,[15] G. Busetto[ff],[40] P. Bussey,[19] A. Buzatu,[31] A. Calamba,[10] C. Calancha,[29] S. Camarda,[4] M. Campanelli,[28] M. Campbell,[32] F. Canelli[11],[15] B. Carls,[22] D. Carlsmith,[56] R. Carosi,[42] S. Carrillo[m],[16] S. Carron,[15] B. Casal[k],[9] M. Casarsa,[50] A. Castro[ee],[6] P. Catastini,[20] D. Cauz,[50] V. Cavaliere,[22] M. Cavalli-Sforza,[4] A. Cerri[f],[26] L. Cerrito[s],[28] Y.C. Chen,[1] M. Chertok,[7] G. Chiarelli,[42] G. Chlachidze,[15] F. Chlebana,[15] K. Cho,[25] D. Chokheli,[13] W.H. Chung,[56] Y.S. Chung,[45] M.A. Ciocci[hh],[42] A. Clark,[18] C. Clarke,[55] G. Compostella[ff],[40] M.E. Convery,[15] J. Conway,[7] M.Corbo,[15] M. Cordelli,[17] C.A. Cox,[7] D.J. Cox,[7] F. Crescioli[gg],[42] J. Cuevas[z],[9] R. Culbertson,[15] D. Dagenhart,[15] N. d'Ascenzo[w],[15] M. Datta,[15] P. de Barbaro,[45] M. Dell'Orso[gg],[42] L. Demortier,[46] M. Deninno,[6] F. Devoto,[21] M. d'Errico[ff],[40] A. Di Canto[gg],[42] B. Di Ruzza,[15] J.R. Dittmann,[5] M. D'Onofrio,[27] S. Donati[gg],[42] P. Dong,[15] M. Dorigo,[50] T. Dorigo,[40] K. Ebina,[54] A. Elagin,[49] A. Eppig,[32] R. Erbacher,[7] S. Errede,[22] N. Ershaidat[dd],[15] R. Eusebi,[49] S. Farrington,[39] M. Feindt,[24] J.P. Fernandez,[29] R. Field,[16] G. Flanagan[u],[15] R. Forrest,[7] M.J. Frank,[5] M. Franklin,[20] J.C. Freeman,[15] Y. Funakoshi,[54] I. Furic,[16] M. Gallinaro,[46] J.E. Garcia,[18] A.F. Garfinkel,[44] P. Garosi[hh],[42] H. Gerberich,[22] E. Gerchtein,[15] S. Giagu,[47] V. Giakoumopoulou,[3] P. Giannetti,[42] K. Gibson,[43] C.M. Ginsburg,[15] N. Giokaris,[3] P. Giromini,[17] G. Giurgiu,[23] V. Glagolev,[13] D. Glenzinski,[15] M. Gold,[35] D. Goldin,[49] N. Goldschmidt,[16] A. Golossanov,[15] G. Gomez,[9] G. Gomez-Ceballos,[30] M. Goncharov,[30] O. González,[29] I. Gorelov,[35] A.T. Goshaw,[14] K. Goulianos,[46] S. Grinstein,[4] C. Grosso-Pilcher,[11] R.C. Group[53],[15] J. Guimaraes da Costa,[20] S.R. Hahn,[15] E. Halkiadakis,[48] A. Hamaguchi,[38] J.Y. Han,[45] F. Happacher,[17] K. Hara,[51] D. Hare,[48] M. Hare,[52] R.F. Harr,[55] K. Hatakeyama,[5] C. Hays,[39] M. Heck,[24] J. Heinrich,[41] M. Herndon,[56] S. Hewamanage,[5] A. Hocker,[15] W. Hopkins[g],[15] D. Horn,[24] S. Hou,[1] R.E. Hughes,[36] M. Hurwitz,[11] U. Husemann,[57] N. Hussain,[31] M. Hussein,[33] J. Huston,[33] G. Introzzi,[42] M. Iori[jj],[47] A. Ivanov[p],[7] E. James,[15] D. Jang,[10] B. Jayatilaka,[14] E.J. Jeon,[25] S. Jindariani,[15] M. Jones,[44] K.K. Joo,[25] S.Y. Jun,[10] T.R. Junk,[15] T. Kamon[25],[49] P.E. Karchin,[55] A. Kasmi,[5] Y. Kato[o],[38] W. Ketchum,[11] J. Keung,[41] V. Khotilovich,[49] B. Kilminster,[15] D.H. Kim,[25] H.S. Kim,[25] J.E. Kim,[25] M.J. Kim,[17] S.B. Kim,[25] S.H. Kim,[51] Y.K. Kim,[11] Y.J. Kim,[25] N. Kimura,[54] M. Kirby,[15] S. Klimenko,[16] K. Knoepfel,[15] K. Kondo*,[54] D.J. Kong,[25] J. Konigsberg,[16] A.V. Kotwal,[14] M. Kreps,[24] J. Kroll,[41] D. Krop,[11] M. Kruse,[14] V. Krutelyov[c],[49] T. Kuhr,[24] M. Kurata,[51] S. Kwang,[11] A.T. Laasanen,[44] S. Lami,[42] S. Lammel,[15] M. Lancaster,[28] R.L. Lander,[7] K. Lannon[y],[36] A. Lath,[48] G. Latino[hh],[42] T. LeCompte,[2] E. Lee,[49] H.S. Lee[q],[11] J.S. Lee,[25] S.W. Lee[bb],[49] S. Leo[gg],[42] S. Leone,[42] J.D. Lewis,[15] A. Limosani[t],[14] C.-J. Lin,[26] M. Lindgren,[15] E. Lipeles,[41] A. Lister,[18] D.O. Litvintsev,[15] C. Liu,[43] H. Liu,[53] Q. Liu,[44] T. Liu,[15] S. Lockwitz,[57] A. Loginov,[57] D. Lucchesi[ff],[40] J. Lueck,[24] P. Lujan,[26] P. Lukens,[15] G. Lungu,[46] J. Lys,[26] R. Lysak[e],[12] R. Madrak,[15] K. Maeshima,[15] P. Maestro[hh],[42] S. Malik,[46] G. Manca[a],[27] A. Manousakis-Katsikakis,[3] F. Margaroli,[47] C. Marino,[24] M. Martínez,[4] P. Mastrandrea,[47] K. Matera,[22] M.E. Mattson,[55] A. Mazzacane,[15] P. Mazzanti,[6] K.S. McFarland,[45] P. McIntyre,[49] R. McNulty[j],[27] A. Mehta,[27] P. Mehtala,[21] C. Mesropian,[46] T. Miao,[15] D. Mietlicki,[32] A. Mitra,[1] H. Miyake,[51] S. Moed,[15] N. Moggi,[6] M.N. Mondragon[m],[15] C.S. Moon,[25] R. Moore,[15] M.J. Morello[ii],[42] J. Morlock,[24] P. Movilla Fernandez,[15] A. Mukherjee,[15] Th. Muller,[24] P. Murat,[15] M. Mussini[ee],[6] J. Nachtman[n],[15] Y. Nagai,[51] J. Naganoma,[54] I. Nakano,[37] A. Napier,[52] J. Nett,[49] C. Neu,[53] M.S. Neubauer,[22] J. Nielsen[d],[26] L. Nodulman,[2] S.Y. Noh,[25] O. Norniella,[22] L. Oakes,[39] S.H. Oh,[14] Y.D. Oh,[25] I. Oksuzian,[53] T. Okusawa,[38] R. Orava,[21] L. Ortolan,[4] S. Pagan Griso[ff],[40] C. Pagliarone,[50] E. Palencia[f],[9] V. Papadimitriou,[15] A.A. Paramonov,[2] J. Patrick,[15] G. Pauletta[kk],[50] M. Paulini,[10] C. Paus,[30] D.E. Pellett,[7] A. Penzo,[50] T.J. Phillips,[14] G. Piacentino,[42] E. Pianori,[41] J. Pilot,[36] K. Pitts,[22] C. Plager,[8] L. Pondrom,[56] S. Poprocki[g],[15] K. Potamianos,[44] F. Prokoshin[cc],[13] A. Pranko,[26] F. Ptohos[h],[17] G. Punzi[gg],[42] A. Rahaman,[43] V. Ramakrishnan,[56] N. Ranjan,[44] I. Redondo,[29] P. Renton,[39] M. Rescigno,[47] T. Riddick,[28] F. Rimondi[ee],[6] L. Ristori[42],[15] A. Robson,[19] T. Rodrigo,[9] T. Rodriguez,[41] E. Rogers,[22] S. Rolli[i],[52] R. Roser,[15] F. Ruffini[hh],[42] A. Ruiz,[9] J. Russ,[10] V. Rusu,[15] A. Safonov,[49] W.K. Sakumoto,[45] Y. Sakurai,[54] L. Santi[kk],[50] K. Sato,[51] V. Saveliev[w],[15] A. Savoy-Navarro[aa],[15] P. Schlabach,[15] A. Schmidt,[24] E.E. Schmidt,[15] T. Schwarz,[15] L. Scodellaro,[9] A. Scribano[hh],[42] F. Scuri,[42] S. Seidel,[35] Y. Seiya,[38] A. Semenov,[13] F. Sforza[hh],[42] S.Z. Shalhout,[7] T. Shears,[27] P.F. Shepard,[43] M. Shimojima[v],[51] M. Shochet,[11] I. Shreyber-Tecker,[34] A. Simonenko,[13] P. Sinervo,[31] K. Sliwa,[52]

J.R. Smith,[7] F.D. Snider,[15] A. Soha,[15] V. Sorin,[4] H. Song,[43] P. Squillacioti[hh],[42] M. Stancari,[15] R. St. Denis,[19] B. Stelzer,[31] O. Stelzer-Chilton,[31] D. Stentz[x],[15] J. Strologas,[35] G.L. Strycker,[32] Y. Sudo,[51] A. Sukhanov,[15] I. Suslov,[13] K. Takemasa,[51] Y. Takeuchi,[51] J. Tang,[11] M. Tecchio,[32] P.K. Teng,[1] J. Thom[g],[15] J. Thome,[10] G.A. Thompson,[22] E. Thomson,[41] D. Toback,[49] S. Tokar,[12] K. Tollefson,[33] T. Tomura,[51] D. Tonelli,[15] S. Torre,[17] D. Torretta,[15] P. Totaro,[40] M. Trovato[ii],[42] F. Ukegawa,[51] S. Uozumi,[25] A. Varganov,[32] F. Vázquez[m],[16] G. Velev,[15] C. Vellidis,[15] M. Vidal,[44] I. Vila,[9] R. Vilar,[9] J. Vizán,[9] M. Vogel,[35] G. Volpi,[17] P. Wagner,[41] R.L. Wagner,[15] T. Wakisaka,[38] R. Wallny,[8] S.M. Wang,[1] A. Warburton,[31] D. Waters,[28] W.C. Wester III,[15] D. Whiteson[b],[41] A.B. Wicklund,[2] E. Wicklund,[15] S. Wilbur,[11] F. Wick,[24] H.H. Williams,[41] J.S. Wilson,[36] P. Wilson,[15] B.L. Winer,[36] P. Wittich[g],[15] S. Wolbers,[15] H. Wolfe,[36] T. Wright,[32] X. Wu,[18] Z. Wu,[5] K. Yamamoto,[38] D. Yamato,[38] T. Yang,[15] U.K. Yang[r],[11] Y.C. Yang,[25] W.-M. Yao,[26] G.P. Yeh,[15] K. Yi[n],[15] J. Yoh,[15] K. Yorita,[54] T. Yoshida[l],[38] G.B. Yu,[14] I. Yu,[25] S.S. Yu,[15] J.C. Yun,[15] A. Zanetti,[50] Y. Zeng,[14] C. Zhou,[14] and S. Zucchelli[ee][6]

(CDF Collaboration[†])

[1]*Institute of Physics, Academia Sinica, Taipei, Taiwan 11529, Republic of China*
[2]*Argonne National Laboratory, Argonne, Illinois 60439, USA*
[3]*University of Athens, 157 71 Athens, Greece*
[4]*Institut de Fisica d'Altes Energies, ICREA, Universitat Autonoma de Barcelona, E-08193, Bellaterra (Barcelona), Spain*
[5]*Baylor University, Waco, Texas 76798, USA*
[6]*Istituto Nazionale di Fisica Nucleare Bologna,* [ee]*University of Bologna, I-40127 Bologna, Italy*
[7]*University of California, Davis, Davis, California 95616, USA*
[8]*University of California, Los Angeles, Los Angeles, California 90024, USA*
[9]*Instituto de Fisica de Cantabria, CSIC-University of Cantabria, 39005 Santander, Spain*
[10]*Carnegie Mellon University, Pittsburgh, Pennsylvania 15213, USA*
[11]*Enrico Fermi Institute, University of Chicago, Chicago, Illinois 60637, USA*
[12]*Comenius University, 842 48 Bratislava, Slovakia; Institute of Experimental Physics, 040 01 Kosice, Slovakia*
[13]*Joint Institute for Nuclear Research, RU-141980 Dubna, Russia*
[14]*Duke University, Durham, North Carolina 27708, USA*
[15]*Fermi National Accelerator Laboratory, Batavia, Illinois 60510, USA*
[16]*University of Florida, Gainesville, Florida 32611, USA*
[17]*Laboratori Nazionali di Frascati, Istituto Nazionale di Fisica Nucleare, I-00044 Frascati, Italy*
[18]*University of Geneva, CH-1211 Geneva 4, Switzerland*
[19]*Glasgow University, Glasgow G12 8QQ, United Kingdom*
[20]*Harvard University, Cambridge, Massachusetts 02138, USA*
[21]*Division of High Energy Physics, Department of Physics,*
University of Helsinki and Helsinki Institute of Physics, FIN-00014, Helsinki, Finland
[22]*University of Illinois, Urbana, Illinois 61801, USA*
[23]*The Johns Hopkins University, Baltimore, Maryland 21218, USA*
[24]*Institut für Experimentelle Kernphysik, Karlsruhe Institute of Technology, D-76131 Karlsruhe, Germany*
[25]*Center for High Energy Physics: Kyungpook National University,*
Daegu 702-701, Korea; Seoul National University, Seoul 151-742,
Korea; Sungkyunkwan University, Suwon 440-746,
Korea; Korea Institute of Science and Technology Information,
Daejeon 305-806, Korea; Chonnam National University, Gwangju 500-757,
Korea; Chonbuk National University, Jeonju 561-756, Korea
[26]*Ernest Orlando Lawrence Berkeley National Laboratory, Berkeley, California 94720, USA*
[27]*University of Liverpool, Liverpool L69 7ZE, United Kingdom*
[28]*University College London, London WC1E 6BT, United Kingdom*
[29]*Centro de Investigaciones Energeticas Medioambientales y Tecnologicas, E-28040 Madrid, Spain*
[30]*Massachusetts Institute of Technology, Cambridge, Massachusetts 02139, USA*
[31]*Institute of Particle Physics: McGill University, Montréal, Québec,*
Canada H3A 2T8; Simon Fraser University, Burnaby, British Columbia,
Canada V5A 1S6; University of Toronto, Toronto, Ontario,
Canada M5S 1A7; and TRIUMF, Vancouver, British Columbia, Canada V6T 2A3
[32]*University of Michigan, Ann Arbor, Michigan 48109, USA*
[33]*Michigan State University, East Lansing, Michigan 48824, USA*
[34]*Institution for Theoretical and Experimental Physics, ITEP, Moscow 117259, Russia*
[35]*University of New Mexico, Albuquerque, New Mexico 87131, USA*
[36]*The Ohio State University, Columbus, Ohio 43210, USA*
[37]*Okayama University, Okayama 700-8530, Japan*
[38]*Osaka City University, Osaka 588, Japan*
[39]*University of Oxford, Oxford OX1 3RH, United Kingdom*
[40]*Istituto Nazionale di Fisica Nucleare, Sezione di Padova-Trento,* [ff]*University of Padova, I-35131 Padova, Italy*

[41] University of Pennsylvania, Philadelphia, Pennsylvania 19104, USA
[42] Istituto Nazionale di Fisica Nucleare Pisa, [gg] University of Pisa,
[hh] University of Siena and [ii] Scuola Normale Superiore, I-56127 Pisa, Italy
[43] University of Pittsburgh, Pittsburgh, Pennsylvania 15260, USA
[44] Purdue University, West Lafayette, Indiana 47907, USA
[45] University of Rochester, Rochester, New York 14627, USA
[46] The Rockefeller University, New York, New York 10065, USA
[47] Istituto Nazionale di Fisica Nucleare, Sezione di Roma 1,
[jj] Sapienza Università di Roma, I-00185 Roma, Italy
[48] Rutgers University, Piscataway, New Jersey 08855, USA
[49] Texas A&M University, College Station, Texas 77843, USA
[50] Istituto Nazionale di Fisica Nucleare Trieste/Udine,
I-34100 Trieste, [kk] University of Udine, I-33100 Udine, Italy
[51] University of Tsukuba, Tsukuba, Ibaraki 305, Japan
[52] Tufts University, Medford, Massachusetts 02155, USA
[53] University of Virginia, Charlottesville, Virginia 22906, USA
[54] Waseda University, Tokyo 169, Japan
[55] Wayne State University, Detroit, Michigan 48201, USA
[56] University of Wisconsin, Madison, Wisconsin 53706, USA
[57] Yale University, New Haven, Connecticut 06520, USA

Using data from $p\bar{p}$ collisions at $\sqrt{s} = 1.96\,\text{TeV}$ recorded by the CDF II detector at the Fermilab Tevatron, we present improved measurements of the masses and first measurements of natural widths of the four bottom baryon resonance states Σ_b^+, Σ_b^{*+} and Σ_b^-, Σ_b^{*-}. These states are fully reconstructed in their decay modes to $\Lambda_b^0\pi^\pm$ where $\Lambda_b^0 \to \Lambda_c^+\pi^-$ with $\Lambda_c^+ \to pK^-\pi^+$. The analysis is based on a data sample corresponding to an integrated luminosity $6.0\,\text{fb}^{-1}$ collected by a trigger on tracks displaced from the $p\bar{p}$ interaction point.

PACS numbers: 14.20.Mr, 13.30Eg, 14.65.Fy

I. INTRODUCTION

Baryons with a heavy quark Q as the "nucleus" and a light diquark q_1q_2 as the two orbiting "electrons" can be viewed as the "helium atoms" of quantum chromodynamics (QCD). The heavy quark in the baryon may be used as a probe of confinement which allows the study of non-perturbative QCD in a different regime from that of the light baryons.

Remarkable achievements in the theory of heavy quark hadrons were made when it was realized that a single heavy quark Q with mass $m_Q \gg \Lambda_{\text{QCD}}$ in the heavy hadron H_Q can be considered as a static color source in the hadron's rest frame [1]. Based on this conjecture the light diquark properties of the charm baryon Λ_c^+ (Σ_c) and its bottom partner Λ_b^0 (Σ_b) can be related by an approximate $SU(2)$ symmetry due to $c \leftrightarrow b$ quark exchange. Another symmetry emerges because the spin S_Q degree of freedom decouples from the gluon field. Models exploiting these heavy quark symmetries are grouped as heavy quark effective theories (HQET) [2, 3].

As the spin S_{qq} of a diquark (plus a gluon field) and the spin S_Q of a heavy quark are decoupled in HQET and serve as approximate good quantum numbers, heavy baryons can be described by the quantum numbers S_Q, m_Q, S_{qq}, m_{qq}. Therefore the total spins of the S-wave ($l_{qq} = 0$, no orbital excitation) baryon multiplets can be expressed as the simple sum $J = S_Q + S_{qq}$. Then the singlet Λ_b^0 baryon, with quark content $b[ud]$ according to HQET, has spin of the heavy quark $S_b = \frac{1}{2}^+$. Its flavor antisymmetric $[ud]$ diquark has spin $S_{[ud]} = 0$. Under these conditions the b quark and $[ud]$ make the lowest-lying singlet ground state $J^P = \frac{1}{2}^+$. The partner of the Λ_b^0 baryon in the strange quark sector is Λ^0. The other two states Σ_b and Σ_b^* with quark content $b\{qq\}$, heavy quark spin $S_b = \frac{1}{2}^+$, and spin of the flavor symmetric $\{qq\}$ diquark $S_{\{qq\}} = 1^+$, constitute two isospin $I = 1$ triplets with total spin $J^P = \frac{1}{2}^+$ and $J^P = \frac{3}{2}^+$. These states are the lowest-lying S-wave states that can decay to the singlet Λ_b^0 via strong processes involving soft pion emissions – provided sufficient phase space is available. Σ_b and Σ_b^* are classified as bottom baryon resonant states. The partners of the $\Sigma_b^{(*)}$ states [4] in the strange quark sector are $\Sigma^{(*)}$ baryon resonances, though the $J^P = \frac{1}{2}^+$ Σ states are light enough to decay only weakly or radiatively, and only the $J^P = \frac{3}{2}^+$ states $\Sigma(1385)$ decay strongly via the $\Lambda^0\pi$ mode [5].

Some recent HQET calculations for bottom baryons are available in Ref. [6]. The mass spectra of single heavy quark baryons calculated with HQET in combined expansions in $1/m_Q$ and $1/N_c$ are presented in Ref. [7]. In the potential quark model, the mass differences $m(\Sigma_Q) - m(\Lambda_Q)$ and $m(\Sigma_Q^*) - m(\Sigma_Q)$ are largely due to hyperfine splittings, hence the mass differences scale as $1/m_Q$. Some recent predictions based on potential quark models are found in Ref. [8, 9]. There are striking patterns in the masses and mass differences of known hadrons. Some of these regularities can be understood from known general properties of the interactions of quarks, without spec-

*Deceased
†With visitors from [a]Istituto Nazionale di Fisica Nucleare, Sezione di Cagliari, 09042 Monserrato (Cagliari), Italy, [b]University of CA Irvine, Irvine, CA 92697, USA, [c]University of CA Santa Barbara, Santa Barbara, CA 93106, USA, [d]University of CA Santa Cruz,

ifying the explicit form of the Hamiltonian. Following this minimalist approach, the authors of Ref. [10] use semi-empirical mass formulae to predict the spectra of c- and b- baryons. The non-perturbative formalism of QCD sum rules has been applied within HQET to calculate the mass spectra of the heavy baryons Λ_Q and Σ_Q [11]. Lattice non-relativistic QCD calculations for bottom baryons [12] have been quite successful, though the statistical and systematic uncertainties are typically large and exceed the uncertainties of the experimental measurements.

The mass splittings between members of the $I = 1$ isospin triplets $\Sigma_b^{(*)}$ are predicted to be dominated by the electromagnetic interactions between quarks and by their intrinsic mass differences [13]. Because of electromagnetic effects and the fact that the d quark is heavier than the u quark, the $\Sigma_b^{(*)-}$ states (with composition $b\{dd\}$ *i.e.* all quarks negative) are expected to be heavier than the $\Sigma_b^{(*)+}$ states whose composition is $b\{uu\}$ [14]. No previous experimental measurements of isospin mass splitting of bottom baryons are available.

The description of strong decays of baryon resonances is a difficult theoretical task [15]. A few theoretical calculations [16–18] predict the natural widths of the $\Sigma_b^{(*)}$ states. The widths are expected to be within the range $(4.5 - 13.5)\,\mathrm{MeV}/c^2$ for $\Gamma(\Sigma_b, \frac{1}{2}^+)$, and the range $(8.5 - 18.0)\,\mathrm{MeV}/c^2$ for $\Gamma(\Sigma_b^*, \frac{3}{2}^+)$.

Until recently, direct observation of b-baryons has been limited to the Λ_b^0 reconstructed in its weak decays to $J/\psi\,\Lambda^0$ and $\Lambda_c^+\pi^-$ [5]. The substantially enlarged experimental data sets delivered by the Tevatron allow significant advances in the spectroscopy of heavy quark baryon states. The resonance $\Sigma_b^{(*)}$ states were discovered by CDF [19]. The charged bottom strange baryon Ξ_b^- particle was observed and measured [20–22] by both the CDF and DO Collaborations. Later, both experimental groups reported first observation [23] and then measurement [22] of the bottom doubly strange particle Ω_b^-. Lastly, the neutral partner of Ξ_b^-, the bottom strange baryon Ξ_b^0, was reported for the first time by CDF [24]. Precise measurements of the masses and natural widths of baryon resonances in the charm sector, specifically the $\Sigma_c^{(*)0}$, $\Sigma_c^{(*)++}$, and Λ_c^{*+}, were recently made public by the CDF Collaboration [25].

This study follows the first observation of the $\Sigma_b^{(*)}$ states [19]. We confirm the observation of those states using a larger data sample, address some criticism [26] regarding the earlier analysis, and add new measurements of properties of the $\Sigma_b^{(*)}$ resonances. In the present analysis, the mass difference spectra for all isospin partner states, $\Sigma_b^{(*)+}$ and $\Sigma_b^{(*)-}$, are determined independently without any mass-difference constraint, unlike in the previous CDF analysis [19]. The background shapes of the experimental spectra are left floating in the fits to avoid systematic uncertainties associated with Monte Carlo models. Using an enlarged data sample, we extract the direct mass difference measurements with smaller statistical and systematic uncertainties than previously. First measurements of the natural widths of the $J^P = \frac{3}{2}^+$ and $J^P = \frac{1}{2}^+$ states are presented. Based on the new mass measurements, we determine the isospin mass splitting for the Σ_b and Σ_b^* isospin $I = 1$ triplets.

Section II provides a brief description of the CDF II detector, the online event selection (trigger) important for this analysis, and the detector simulation. In Sec. III the data selection, analysis requirements, and reconstruction of the signal candidates are described. Section IV discusses the fit model of the final spectra and summarizes the fit results. In Sec. V we estimate the significance of signals extracted from the fits. The systematic uncertainties are discussed in Sec. VI. We present a summary of the measurements and conclusions in Sec. VII.

II. THE CDF II DETECTOR AND SIMULATION

The component of the CDF II detector [27] most relevant to this analysis is the charged particle tracking system. The tracking system operates in a uniform axial magnetic field of 1.4 T generated by a superconducting solenoidal magnet.

The CDF II detector uses a cylindrical coordinate system with z-axis along the nominal proton beam-line, radius r measured from the beam-line and ϕ defined as an azimuthal angle. The transverse plane (r, ϕ) is perpendicular to the z-axis. The polar angle, θ, is measured from the z-axis. The impact-parameter of a charged particle track d_0 is defined as the distance of closest approach of the particle track to the primary vertex in the transverse plane. Transverse momentum, p_{T}, is the component of the particle's momentum projected onto the transverse plane. Pseudorapidity is defined as $\eta \equiv -\ln(\tan(\theta/2))$.

The inner tracking system comprises two silicon detectors: the silicon vertex detector (SVX II) and the intermediate silicon layers (ISL) [28–31]. The SVX II detector consists of microstrip sensors arranged in six cylindrical layers. The innermost part, also referred to as the L00 detector, is a layer of single-sided silicon sensors mounted directly on the beam pipe, 1.5 cm from the proton beam-line. It enhances the transverse impact parameter resolution. Outside this, the five double-sided layers of SVX II provide up to 10 track position measurements. Each of the layers provides an r-ϕ measurement, while three return a measurement along z, and the other two return a measurement along a direction oriented at $\pm 1.2^\circ$ to the z-axis. The SVX II spans the radii between 1.5 cm and 10.6 cm and covers the pseudorapidity range $|\eta| < 2.0$. The SVX II detector provides a vertex resolution of approximately $15\,\mu$m in the transverse plane and $70\,\mu$m along the z-axis. A fine track impact parameter resolution $\sigma_{d_0} \simeq 35\,\mu$m is achieved, where the σ_{d_0} includes an approximately $28\,\mu$m contribution from the actual transverse size of the beam spot. The outermost silicon subdetector, ISL, consists of double-sided layers

at radii 20 cm to 28 cm, providing two or four hits per track depending on the track pseudorapidity within the range $|\eta| < 2.0$ instrumented by the ISL.

A large open cell cylindrical drift chamber, the central outer tracker (COT) [32], completes the CDF detector tracking system. The COT consists of 96 sense wire layers arranged in 8 superlayers of 12 wires each. Four of these superlayers provide axial measurements, and four provide stereo views at $\pm 2°$. The active volume of the COT spans the radial region from 43.4 cm to 132.3 cm. The pseudorapidity range $|\eta| < 1.0$ is covered for tracks passing through all layers of the COT, while for the range out to $1.0 < |\eta| < 2.0$, tracks pass through fewer than the full 96 layers. The trajectory of COT tracks is extrapolated into the SVX II detector, and the tracks are refitted with additional silicon hits consistent with the track extrapolation. The two additional layers of the ISL help to link tracks in the COT to hits in the SVX II. The combined track transverse momentum resolution is $\sigma(p_{\rm T})/p_{\rm T} \simeq 0.07\% \cdot p_{\rm T}\,[\,{\rm GeV}/c]^{-1}$.

The analysis presented here is based on events recorded with a three-tiered trigger system configured to collect large data samples of heavy hadrons decaying through multi-body hadronic channels. We refer to this as the displaced two-track trigger. We use two configurations of this trigger, the "low-$p_{\rm T}$" and the "medium-$p_{\rm T}$" selections. At level 1, the trigger uses information from the hardware extremely fast tracker [33]. The "low-$p_{\rm T}$" configuration of the displaced two-track trigger requires two tracks in the COT with $p_{\rm T} > 2.0\,{\rm GeV}/c$ for each track, and with an opening angle of $|\Delta\phi| < 90°$ between the tracks in the transverse plane. Additionally the track pair scalar sum must satisfy $p_{\rm T1} + p_{\rm T2} > 4.0\,{\rm GeV}/c$. The corresponding criteria imposed in the "medium-$p_{\rm T}$" configuration are $p_{\rm T} > 2.0\,{\rm GeV}/c$ for each track, opening angle $|\Delta\phi| < 135°$, and $p_{\rm T1} + p_{\rm T2} > 5.5\,{\rm GeV}/c$. The level 2 silicon vertex trigger (SVT) [34, 35] associates the track pair from the extremely fast tracker with hits in the SVX II detector and recognizes both tracks using a large look-up table of hit patterns. The SVT repeats the level 1 $p_{\rm T}$ criteria and limits the opening angle to $2° < |\Delta\phi| < 90°$. Only in the case of the medium-$p_{\rm T}$ configuration are the charges of the tracks required to be of opposite sign. Crucially, the SVT imposes a requirement on the transverse impact parameter of each track to be $120\,\mu{\rm m} < d_0 < 1\,{\rm mm}$ given the excellent resolution provided by SVX II. Finally, the distance in the transverse plane between the beam axis and the intersection point of the two tracks projected onto their total transverse momentum is required to be $L_{xy} > 200\,\mu{\rm m}$. The level 3 software trigger uses a full reconstruction of the event with all detector information and confirms the criteria applied at level 2. The trigger criteria applied to the d_0 of each track in the pair and to L_{xy} preferentially select decays of long-lived heavy hadrons over prompt background, ensuring that the data sample is enriched with b-hadrons.

The mass resolution on the $\Sigma_b^{(*)}$ resonances is predicted with a Monte Carlo simulation that generates b quarks according to a next-to-leading order calculation [36] and produces events containing final state hadrons by simulating b-quark fragmentation [37]. Mass values of $5807.8\,{\rm MeV}/c^2$ for Σ_b and $5829.0\,{\rm MeV}/c^2$ for Σ_b^* [19] are used in the Monte Carlo generator. Final state decay processes are simulated with the EVTGEN [38] program, and all simulated b-hadrons are produced without polarization. The generated events are input to the detector and trigger simulation based on GEANT3 [39] and processed through the same reconstruction and analysis algorithms as are used on the data.

III. DATA SAMPLE AND EVENT SELECTION

This analysis is based on data equivalent to 6.0 ${\rm fb}^{-1}$ of $p\overline{p}$ collisions collected with the displaced two-track trigger between March 2002 and February 2010. We study $\Sigma_b^{(*)}$ resonances in the exclusive fully reconstructed strong decay mode $\Sigma_b^{(*)\pm} \to \Lambda_b^0 \pi_s^\pm$, where the low momentum pion $\pi_s^\pm$ is produced near kinematical threshold [40]. The Λ_b^0 decays to $\Lambda_c^+ \pi_b^-$ with a prompt pion π_b^- produced in the weak decay. This is followed by the weak decay $\Lambda_c^+ \to pK^-\pi^+$.

To reconstruct the parent baryons, the tracks of charged particles are combined in a kinematic fit to form candidates. The following two complementary quantities defined in the plane transverse to the beam line and relating the decay path of baryons to their points of origin are used: the proper decay time of the baryon candidate h expressed in length units $ct(h)$, and the impact parameter $d_0(h)$. Specifically,

$$ct(h) = L_{xy}(h) \cdot \frac{M(h) \cdot c}{p_{\rm T}(h)}\ , \qquad (1)$$

where $L_{xy}(h)$ is expressed in length units and defined as the projection onto $\vec{p}_T(h)$ of the vector connecting the primary vertex to the heavy baryon decay vertex in the transverse plane. The impact parameter $d_0(h)$ of the candidate is defined as the distance of closest approach of the candidate to the primary vertex in the transverse plane. An event-specific primary interaction vertex is used in the calculation of the $ct(h)$ and $d_0(h)$ quantities. The measurement uncertainties σ_{ct} and σ_{d_0} originate from the track parameter uncertainties and the uncertainty on the primary vertex.

A. Reconstruction of the Λ_b^0 candidates

The analysis begins with reconstruction of the $\Lambda_c^+ \to pK^-\pi^+$ decay by fitting three tracks to a common vertex. The invariant mass of the Λ_c^+ candidate is required to be within $\pm 18\,{\rm MeV}/c^2$ of the world-average Λ_c^+ mass [5]. The momentum vector of the Λ_c^+ candidate is then extrapolated to intersect with a fourth pion track, the

π_b^--candidate, to form the $\Lambda_b^0 \to \Lambda_c^+\pi_b^-$ candidate vertex. The Λ_b^0 vertex is subjected to a three-dimensional kinematic fit with the Λ_c^+ candidate mass constrained to its world average value [5]. The probability of the constrained Λ_b^0 vertex fit must exceed 0.01%. Standard quality requirements are applied to each track, and only tracks with $p_{\rm T} > 400\,{\rm MeV}/c$ are used. No particle identification is used in this analysis. At this stage of the reconstruction, at least two tracks among the p, K^-, π^+, and π_b^- are required to fulfill the level 2 (SVT) trigger requirements in order to confirm the displaced two-track trigger decision.

To suppress prompt backgrounds from the primary interaction, the decay vertex of the Λ_b^0 is required to be distinct from the primary vertex. To achieve this, cuts on $ct(\Lambda_b^0)$ and its significance $ct(\Lambda_b^0)/\sigma_{ct}$ are applied. We require the Λ_c^+ vertex to be close to the Λ_b^0 vertex by applying cuts on $ct(\Lambda_c^+)$ where the corresponding $L_{xy}(\Lambda_c^+)$ is calculated with respect to the Λ_b^0 vertex. To reduce combinatorial background and contributions from partially reconstructed decays, we require Λ_b^0 candidates to point to the primary vertex and the impact parameter $d_0(\Lambda_b^0)$ to be small. The choice of analysis requirements to identify $\Lambda_b^0 \to \Lambda_c^+\pi_b^-$ candidates is made using an optimization based on the experimental data only. The figure of merit $S/\sqrt{S+B}$ is used during the optimization, where S and B are the signal and the background under the signal respectively. Both quantities are obtained from fits of the $M(\Lambda_c^+\pi_b^-)$ invariant mass spectrum. Table I summarizes the Λ_b^0 analysis requirements chosen with this optimization procedure. The specified cut on the total $p_{\rm T}$ of the Λ_b^0 candidate confirms the trigger.

TABLE I: Analysis requirements for $\Lambda_b^0 \to \Lambda_c^+\pi_b^-$ reconstruction. The quantity $ct(\Lambda_c^+ \leftarrow \Lambda_b^0)$ is defined analogously to Eq. (1) as the Λ_c^+ proper time where $L_{xy}(\Lambda_c^+)$ is calculated with respect to the Λ_b^0 vertex.

Quantity	Value
$ct(\Lambda_b^0)$	> 200 μm
$ct(\Lambda_b^0)/\sigma_{ct}$	> 12.0
$d_0(\Lambda_b^0)$	< 80 μm
$ct(\Lambda_c^+ \leftarrow \Lambda_b^0)$	> -150 μm
$ct(\Lambda_c^+ \leftarrow \Lambda_b^0)$	< 250 μm
$p_{\rm T}(\pi_b^-)$	> 1.5 GeV/c
$p_{\rm T}(\Lambda_b^0)$	> 4.0 GeV/c
Prob(χ^2_{3D}) of Λ_b^0 vertex fit	$> 0.01\%$

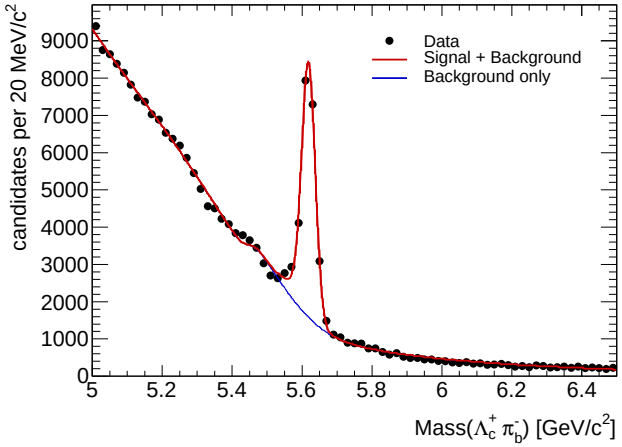

FIG. 1: The invariant mass distribution of $\Lambda_b^0 \to \Lambda_c^+\pi_b^-$ candidates with the projection of a mass fit overlaid.

Figure 1 shows a prominent Λ_b^0 signal in the $M(\Lambda_c^+\pi_b^-)$ invariant mass distribution, reconstructed using the optimized criteria. A binned maximum likelihood fit finds a signal of approximately 16 300 candidates at the expected Λ_b^0 mass, with a signal to background ratio around 1.8. The fit model describing the invariant mass distribution comprises the Gaussian $\Lambda_b^0 \to \Lambda_c^+\pi_b^-$ signal on top of a background shaped by several contributions. Random four-track combinations dominating the right sideband are modeled with an exponentially decreasing function. Coherent sources populate the left sideband and leak under the signal. These include reconstructed B mesons which pass the $\Lambda_b^0 \to \Lambda_c^+\pi_b^-$ selection criteria, partially reconstructed Λ_b^0 decays, and fully reconstructed Λ_b^0 decays other than $\Lambda_c^+\pi_b^-$ (*e.g.* $\Lambda_b^0 \to \Lambda_c^+K^-$). Shapes and functions representing the physical background sources in the fit model are derived and fixed with Monte Carlo simulations. Their normalizations are constrained to branching ratios that are either measured (for B meson decays, reconstructed within the same $\Lambda_c^+\pi_b^-$ sample) or theoretically predicted (for Λ_b^0 decays) [19, 41].

B. Reconstruction of $\Sigma_b^{(*)\pm}$ candidates

To reconstruct the $\Sigma_b^{(*)\pm} \to \Lambda_b^0\pi_s^\pm$ candidates, each $\Lambda_c^+\pi_b^-$ candidate with invariant mass within the Λ_b^0 signal region, $(5.561,\ 5.677)\,{\rm GeV}/c^2$, is combined with one of the tracks remaining in the event with transverse momentum down to $200\,{\rm MeV}/c^2$ and pion mass hypothesis assigned. The Λ_b^0 candidate mass range is based on fit results and covers ± 3 fit uncertainties σ_m around the Λ_b^0 mass peak from fit shown at Fig. 1. To increase the efficiency for reconstructing $\Sigma_b^{(*)\pm}$ decays near the kinematic threshold, minimum acceptable COT and SVX II hit requirements are imposed on $\pi_s^\pm$ tracks, and only tracks with a valid track fit and error matrix are accepted.

Random combinations of Λ_b^0 signal candidates with $\pi_s^\pm$ tracks constitute the dominant background to the $\Sigma_b^{(*)\pm} \to \Lambda_b^0\pi_s^\pm$ signal. The remaining backgrounds are random combinations of soft tracks with B mesons reconstructed as Λ_b^0 baryons, and combinatorial background events [19]. To reduce the background level, a kinematic

TABLE II: $\Sigma_b^{(*)\pm}$ candidate selection requirements.

Quantity	Value
$m(\Lambda_c^+\pi_b^-)$	$\in (5.561,\ 5.677)\,\mathrm{GeV}/c^2$
$d_0(\pi_s^\pm)$	< 0.1 cm
$p_\mathrm{T}(\pi_s^\pm)$	> 200 MeV/c
$d_0(\pi_s^\pm)/\sigma_{d_0}$	< 3.0
$p_\mathrm{T}(\pi_s^\pm)$	$< p_\mathrm{T}(\pi_b^-)$
$p_\mathrm{T}(\Sigma_b^{(*)\pm})$	> 4.0 GeV/c

fit is applied to the resulting combinations of Λ_b^0 candidates and soft pion tracks $\pi_s^\pm$ to constrain them to originate from a common point. Furthermore, since the bottom baryon resonance originates and decays at the primary vertex the soft pion track is required to point back to the primary vertex, specifically, the impact parameter significance $d_0(\pi_s^\pm)/\sigma_{d_0}$ must not exceed 3. The transverse momentum of the soft pion is required to be smaller than the p_T of the π_b^- from the Λ_b^0 weak decay. As the transverse momentum of the π_b^- is already above $1.5\,\mathrm{GeV}/c$ (Table I) the condition imposed on the soft pion p_T has 100% efficiency. The $\Sigma_b^{(*)\pm}$ candidate selection requirements are summarized in Table II. The cut on the total p_T of the $\Sigma_b^{(*)\pm}$ candidate confirms the trigger.

IV. DETERMINATION OF RESONANCE PROPERTIES

The analysis of the $\Sigma_b^{(*)\pm}$ mass distributions is performed using the mass difference

$$Q = m(\Lambda_b^0\pi_s^\pm) - m(\Lambda_b^0) - m_\pi\ , \tag{2}$$

where m_π is the known charged pion mass [5] and $m(\Lambda_b^0)$ is the reconstructed $\Lambda_c^+\pi_b^-$ invariant mass. The mass resolution of the Λ_b^0 signal and most of the systematic uncertainties cancel in the mass difference spectrum. The $\Sigma_b^\pm$ and $\Sigma_b^{*\pm}$ signals are reconstructed as two narrow structures in the Q-value spectrum. The properties, yields, and significance of the resonance candidates are obtained by performing unbinned maximum likelihood fits on the mass difference spectra.

The shapes of the $\Sigma_b^{(*)\pm}$ resonances are each modeled with a non-relativistic Breit-Wigner function. Since the soft pion in $\Sigma_b^{(*)\pm}$ strong decay modes is emitted in a P-wave, the width of the Breit-Wigner function is modified following an approach proposed in Ref. [42] which has been used in analyses of Σ_c baryons [43, 44]. The width is factorized as

$$\Gamma(Q; Q_0, \Gamma_0) = \Gamma_0 \cdot \left(\frac{p^*_{\pi_s}}{p^{*0}_{\pi_s}}\right)^3 , \tag{3}$$

where Q_0 is the mass difference at the resonance pole; $p^*_{\pi_s}$ and $p^{*0}_{\pi_s}$ are the momenta of the soft pion in the $\Sigma_b^{(*)\pm}$ rest frame, off and on the resonance pole respectively; and Γ_0 is the corrected width. The soft pion momenta are calculated based on two-body decay kinematics [5]. Both Q_0 and Γ_0 are floating fit parameters.

The Breit-Wigner function is convoluted with the detector resolution which is described by a narrow core Gaussian plus a broad Gaussian. Their widths σ_n and σ_w and relative weights g_n and $(1-g_n)$ are calculated from the CDF full Monte Carlo simulation. Numerical convolution is necessary because the modified width depends on the mass. The effects of imperfect modeling in the simulation are discussed in Sec. VI.

We use a kinematically motivated model for the background described by a second order polynomial modulated with a threshold square root-like term,

$$\begin{aligned}\mathcal{BG}(Q; m_T, C, b_1, b_2) \ &= \sqrt{(Q+m_\pi)^2 \ - \ {m_T}^2}\times \\ &\quad \mathcal{P}^2(Q; C, b_1, b_2)\,,\end{aligned} \tag{4}$$

where C, b_1, and b_2 are the second order $\mathcal{P}^2$ polynomial coefficients and m_T is a threshold fixed to $0.140\,\mathrm{GeV}/c^2$, the mass of the pion. The threshold term is used to describe combinatorial background to two-body resonance decays near the threshold when the signals are reconstructed in mass difference spectra.

The full model for the Q-value spectra of all isospin partner states $\Sigma_b^{(*)+}$ and $\Sigma_b^{(*)-}$ describes two narrow structures on top of a smooth background with a threshold. The negative logarithm of the extended likelihood function (NLL) is minimized over the unbinned set of Q-values observed for N candidates in data:

$$-\log(\mathcal{L}) \ = \ -\sum_{k=1}^{N} \log(N_1\cdot\mathcal{S}_1 + N_2\cdot\mathcal{S}_2 + N_b\cdot\mathcal{BG}) + (N_1+N_2+N_b) - N\cdot\log(N_1+N_2+N_b)\,. \tag{5}$$

Separate and independent likelihood functions are used for $\Sigma_b^{(*)+}$ and $\Sigma_b^{(*)-}$ candidates. The Q-value spectrum is fit over the range $(0.003,\ 0.210)\,\mathrm{GeV}/c^2$. The effect of this choice is discussed in Sec. VI. The probability

density functions (PDF) in Eq. (5) are defined as follows:

(i) $\mathcal{S}_i = \mathcal{S}(Q; Q_0^i, \Gamma_0^i, \sigma_n^i, g_n^i, \sigma_w^i)$ is the normalized convolution of a Breit-Wigner and a double Gaussian responsible for the Σ_b^+ (Σ_b^-) (i = 1) or Σ_b^{*+} (Σ_b^{*-}) (i = 2) signals. Here Q_0^i is the floating parameter of the pole mass and Γ_0^i is the floating parameter of the natural width. The detector's Gaussian resolution parameters σ_n^i, σ_w^i and g_n^i are set from the Monte Carlo data. Specifically the resolution parameters are set for the Σ_b^+ (Σ_b^-) as $\sigma_n^1 = 1.17\,\mathrm{MeV}/c^2$, $\sigma_w^1 = 2.92\,\mathrm{MeV}/c^2$ with relative weight $g_n^1 = 0.70$ and for the Σ_b^{*+} (Σ_b^{*-}) as $\sigma_n^2 = 1.40\,\mathrm{MeV}/c^2$, $\sigma_w^2 = 3.80\,\mathrm{MeV}/c^2$ with $g_n^2 = 0.73$.

(ii) N_i is the floating yield of the Σ_b^+ (Σ_b^-) (i = 1) or Σ_b^{*+} (Σ_b^{*-}) (i = 2)

(iii) $\mathcal{BG} = \mathcal{BG}(Q; m_T, C, b_1, b_2)$ is the PDF corresponding to the background form in Eq. (4).

(iv) N_b is the floating yield of the background contribution. The sum of fitted yields, $N_1 + N_2 + N_b$, is the Poisson mean value of the total number of candidates N for the particular species Σ_b^+, Σ_b^{*+} or Σ_b^-, Σ_b^{*-} corresponding to isospin triplets Σ_b and Σ_b^*.

The total number of floating parameters in the fit per each pair of isospin partners is nine.

Extensive tests on many statistical trials show that the likelihood fit yields unbiased estimates with proper uncertainties.

The experimental $\Sigma_b^{(*)-}$ and $\Sigma_b^{(*)+}$ Q-value distributions, each fitted with the unbinned likelihoods described above, are shown in Fig. 2 and Fig. 3. The projection of the corresponding likelihood fit is superimposed on each graph. Figures 2 and 3 show clear signals of Σ_b^-, Σ_b^{*-} and Σ_b^+, Σ_b^{*+}, respectively. The pull distributions are shown as bottom plots and are calculated as the residuals of the histogram with respect to the corresponding likelihood fit projection normalized by the data uncertainty. Both pull distributions are evenly distributed around zero with fluctuations of about $\pm 2\sigma$ range. The fit results are given in Table III.

TABLE III: Summary of the results of the fits to the $Q = M(\Lambda_b^0\pi^\pm) - M(\Lambda_b^0) - m_\pi$ spectra. The statistical uncertainties are returned by the unbinned maximum likelihood fits.

State	Q_0-value, MeV/c^2	Natural Width, Γ_0, MeV/c^2	Yield
Σ_b^-	$56.2^{+0.6}_{-0.5}$	$4.9^{+3.1}_{-2.1}$	340^{+90}_{-70}
Σ_b^{*-}	75.8 ± 0.6	$7.5^{+2.2}_{-1.8}$	540^{+90}_{-80}
Σ_b^+	$52.1^{+0.9}_{-0.8}$	$9.7^{+3.8}_{-2.8}$	470^{+110}_{-90}
Σ_b^{*+}	72.8 ± 0.7	$11.5^{+2.7}_{-2.2}$	800^{+110}_{-100}

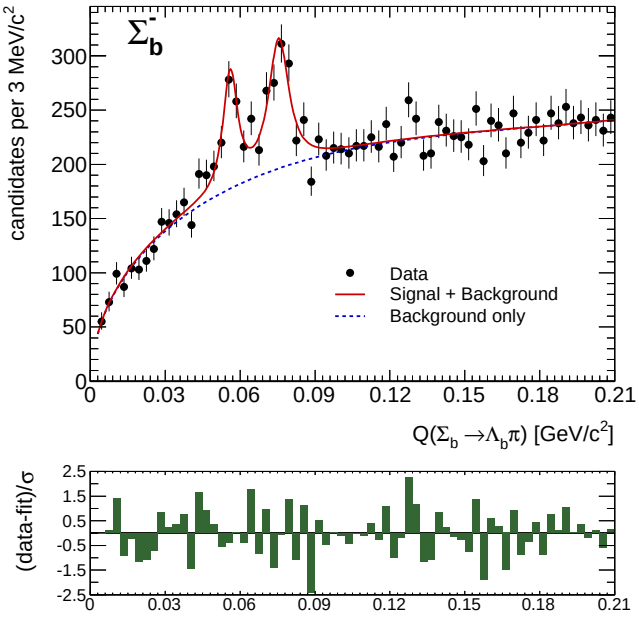

FIG. 2: The Q-value spectrum for $\Sigma_b^{(*)-}$ candidates, where $Q = M(\Lambda_b^0\pi_s^-) - M(\Lambda_b^0) - m_\pi$, is shown with the projection of the corresponding unbinned likelihood fit superimposed. The pull distribution of the fit is shown in the bottom plot.

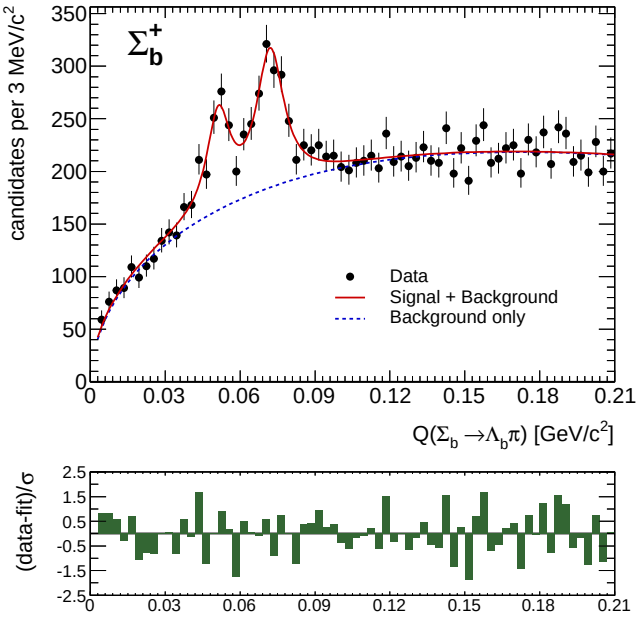

FIG. 3: The Q-value spectrum for $\Sigma_b^{(*)+}$ candidates, where $Q = M(\Lambda_b^0\pi_s^+) - M(\Lambda_b^0) - m_\pi$, is shown with the projection of the corresponding unbinned likelihood fit superimposed. The pull distribution of the fit is shown in the bottom plot.

V. SIGNAL SIGNIFICANCE

The significance of the signals is analyzed using a log-likelihood ratio statistic [45, 46],

$$D = -2 \cdot \log \frac{\mathcal{L}_0}{\mathcal{L}_1} = -2 \cdot \Delta(\log \mathcal{L}) \,. \quad (6)$$

We define a hypothesis $\mathcal{H}_1$ corresponding to the observation of Σ_b^-, Σ_b^{*-} or Σ_b^+, Σ_b^{*+} signals on top of the background. The $\mathcal{H}_1$ hypothesis is described by the likelihood $\mathcal{L}_1$; see Eq. 5. The various null hypotheses, each identified with $\mathcal{H}_0$ and nested to $\mathcal{H}_1$ correspond to a few different less complex scenarios described by the likelihood $\mathcal{L}_0$. Eq. (6) is used to predict the χ^2 to derive p-values for observing a deviation as large as is in our data or larger, assuming $\mathcal{H}_0$ is true. The number of degrees of freedom of the χ^2 equals the difference $\Delta N_{\rm dof}$ in the number degrees of freedom between the $\mathcal{H}_1$ and $\mathcal{H}_0$ hypotheses in each case. We consider the following types of $\mathcal{H}_0$ to estimate the significance of the two-peak signal structure and of individual peaks of the observed $\Sigma_b^{(*)-}$ and $\Sigma_b^{(*)+}$ states:

(i) A single enhancement is observed anywhere in the fit range. The corresponding likelihood $\mathcal{L}_0$ includes only a single peak PDF on top of the background form in Eq. (4), the same as for the $\mathcal{L}_1$. The difference in the number of degrees of freedom is $\Delta N_{\rm dof} = 3$. The width Γ_0 floats in the fit over the wide range $(1,\, 70)\,{\rm MeV}/c^2$. The position of the enhancement Q_0 is allowed to be anywhere within the default fit range. We test the case in which the observed two narrow structures could be an artifact of a wide bump where a few bins fluctuated down to the background level. This particular null hypothesis is found to be the least unlikely to produce the observed data as a fluctuation.

(ii) The signal Σ_b^* is observed but the Σ_b is missed. The number of free parameters is changed by 4. We impose a loose requirement on the existence of the second peak, Σ_b^* fixing only the width of Σ_b^* to the expected theoretical value of $12\,{\rm MeV}/c^2$ [17]. We let the fitter find the Σ_b^* position within the default fit range.

(iii) The signal Σ_b is observed but the Σ_b^* is missed. This null hypothesis is similar to the previous one. The width of the Σ_b is fixed to $7\,{\rm MeV}/c^2$ [17].

(iv) Neither the Σ_b nor the Σ_b^* is observed, and the $\mathcal{H}_0$ hypothesis is the default background model used in $\mathcal{L}_1$. We consider the case in which the smooth background fluctuates to two narrow structures corresponding to the $\mathcal{H}_1$ hypothesis. The difference in the number of degrees of freedom is 6.

In addition to all the cases considered above, we introduce a further in which the $\mathcal{H}_1$ hypothesis corresponds to any single wide enhancement considered in (i) while the $\mathcal{H}_0$ hypothesis is the default background considered in (iv). This special test determines the significance of the single enhancement with respect to pure background.

TABLE IV: The results of comparison of the $\Sigma_b^{(*)-}$ and $\Sigma_b^{(*)+}$ signal $\mathcal{H}_1$ hypothesis with several null $\mathcal{H}_0$ hypotheses. N_σ is the calculated number of Gaussian standard deviations based on Prob(χ^2).

$\mathcal{H}_0$	States	Prob(χ^2)	N_σ	$\mathcal{H}_1$
Any single wide	$\Sigma_b^{(*)-}$	$\approx 3.0 \cdot 10^{-11}$	6.7	two narrow
enhancement	$\Sigma_b^{(*)+}$	$\approx 1.5 \cdot 10^{-9}$	6.1	structures
No structures	$\Sigma_b^{(*)-}$	$\approx 1.1 \cdot 10^{-26}$	10.7	any single wide
	$\Sigma_b^{(*)+}$	$\approx 1.2 \cdot 10^{-39}$	13.2	enhancement
No Σ_b, with Σ_b^*,	$\Sigma_b^{(*)-}$	$\approx 2.3 \cdot 10^{-14}$	7.6	two narrow
$\Gamma_{02} = 12\,{\rm MeV}/c^2$	$\Sigma_b^{(*)+}$	$\approx 3.2 \cdot 10^{-15}$	7.9	structures
No Σ_b^*, with Σ_b,	$\Sigma_b^{(*)-}$	$\approx 1.0 \cdot 10^{-23}$	10.0	two narrow
$\Gamma_{01} = 7\,{\rm MeV}/c^2$	$\Sigma_b^{(*)+}$	$\approx 1.0 \cdot 10^{-35}$	12.5	structures
No structures	$\Sigma_b^{(*)-}$	$\approx 2.4 \cdot 10^{-35}$	12.4	two narrow
	$\Sigma_b^{(*)+}$	$\approx 2.0 \cdot 10^{-46}$	14.3	structures

Table IV summarizes the results of these tests. The null hypothesis most likely to resemble our signal is a broad single enhancement fluctuating to the two narrow structures. The result of this study is that both of the observed $\Sigma_b^{(*)-}$ and $\Sigma_b^{(*)+}$ two-peak signal structures are individually preferred by the signal hypothesis $\mathcal{H}_1$ at greater than 6σ significance relative to null hypothesis (i) which in turn is greater than 10σ away from the pure background model. For other null hypotheses tested, the significance is well above 7σ in Gaussian terms.

VI. SYSTEMATIC UNCERTAINTIES

The systematic uncertainties considered in our analysis are the following:

(i) The uncertainty due to the CDF tracker momentum scale.

(ii) The uncertainty due to the resolution model (see Sec. IV) described by the sum of two Gaussians. This source is expected to dominate the systematic uncertainties on width measurements.

(iii) The choice of background model.

(iv) An uncertainty due to the choice of Q-value fit range.

The uncertainties on the measured $\Sigma_b^{(*)}$ mass differences Q_0 due to the CDF tracker momentum scale are es-

timated from the deviation of CDF mass difference measurements of similar resonance states from their world average values. The reference modes are $\Sigma_c^{++} \to \Lambda_c^+\pi_s^+$, $\Sigma_c^0 \to \Lambda_c^+\pi_s^-$, $\Lambda_c^{*+} \to \Lambda_c^+\pi_s^+\pi_s^-$, and $D^{*+} \to D^0\pi_s^+$. We reconstruct them from CDF data and analyze the deviations of the measured Q_0-values from the world-averaged values [5]. The linear extrapolation of the measured offsets versus Q_0 towards our $\Sigma_b^{(*)}$ points gives the expected mass scale uncertainty at our mass difference range.

Following the method used in Ref. [47], the $D^{*+} \to D^0(\to K^-\pi^+)\pi_s^+$ signal peak in the mass difference distribution $m(D^{*+}) - m(D^0)$ has been reconstructed in several bins of soft pion transverse momentum $p_{\rm T}(\pi_s)$ starting with $200\,{\rm MeV}/c^2$ as in the data. Each distribution is subjected to an unbinned maximum likelihood fit with the sum of a Breit-Wigner function convoluted with a double Gaussian function to describe the detector resolution. The background under the D^{*+} signals is described by an empirical function [48, 49]. For each of the $p_{\rm T}(\pi_s)$ bins, the fit determines the D^{*+} widths not exceeding $0.2\,{\rm MeV}/c^2$. Because the D^{*+} natural width is much smaller than the tracking resolution, the value of $0.2\,{\rm MeV}/c^2$ is assigned as a systematic uncertainty on the measured $\Sigma_b^{(*)}$ natural width due to the momentum scale of the CDF tracker.

Unless otherwise specified the systematic uncertainties discussed below are evaluated for the measurable quantities Q_0 and Γ_0 by generation of statistical trials. In each trial, the sample is generated according to the PDF (see Table III) with the nuisance parameters modified by the uncertainty with respect to the default set of parameters. Then the sample is subjected to the unbinned maximum likelihood fit twice, with the default PDF and with the PDF of the modified nuisance parameter set. The responses of both fitters are compared on a trial by trial basis, and their difference is computed. The systematic uncertainty is found from the mean of a Gaussian fit of the distribution of the computed differences.

The statistical uncertainties on the resolution model parameters due to the finite size of the Monte Carlo datasets introduce a systematic uncertainty. Variations of the double Gaussian widths σ_n and σ_w and the weight g_n within their statistical uncertainties returned from the fits of Monte Carlo spectra are propagated into the measurable quantities using the statistical trials.

The CDF tracking simulation does not reproduce with perfect accuracy the tracking resolutions, especially for soft tracks at the kinematic threshold of $\Sigma_b^{(*)}$ decays. To estimate this contribution, we use the $D^{*\pm}$ hadron decay as the reference mode reconstructed down to $p_{\rm T}(\pi_s^\pm) = 200\,{\rm MeV}/c^2$ in the observed and simulated samples. We compare the mass resolution of the reference signal found in data with the one predicted by Monte Carlo simulation. The comparison is made independently for positive $D^{*+} \to D^0\pi_s^+$ and negative $D^{*-} \to \overline{D}^0\pi_s^-$ states, as a function of soft pion $p_{\rm T}$ using early data taking runs of "Period 1" and late runs of "Period 2." Figure 4 shows the comparisons of the narrow core resolution between the data and Monte Carlo both for D^{*+} (left plot) and D^{*-} (right plot). Note that the resolution is stable for data taken in "Period 1" and "Period 2."

The plots show that the CDF Monte Carlo simulation typically underestimates the $D^{*\pm}$ resolutions in the experimental data, *i.e.* $\sigma_n({\rm data}) \lesssim 1.25 \cdot \sigma_n({\rm Monte\ Carlo})$. Similar relations are found for the broad component of the resolution, $\sigma_w({\rm data}) \lesssim 1.40 \cdot \sigma_w({\rm Monte\ Carlo})$. The resolution extracted for the D^{*+} is systematically higher than for the D^{*-} by at most 20% for σ_n and by at most 40% for σ_w. By generating many statistical trials, we calculate this contribution to the systematic uncertainties of the measurable quantities.

To find the systematic uncertainty associated with the choice of background shape, we change our background PDF to the one used for the $D^{*\pm}$ mass difference spectra [48, 49] and compare with the default background PDF.

The uncertainty associated with the fit range is estimated by modifying the low edge from $0.0015\,{\rm GeV}/c^2$ to $0.006\,{\rm GeV}/c^2$. The fitter reveals small biases in this sensitive area and these are assigned as another systematic uncertainty.

The final systematic uncertainties are listed in Table V.

VII. RESULTS AND CONCLUSIONS

The analysis results are arranged in Table VI. From the measured $\Sigma_b^{(*)\pm}$ Q-values we extract the absolute masses using the world average value of the $\pi^\pm$ mass [5] and the CDF mass measurement for the Λ_b^0 obtained in an independent sample [50], which is $m(\Lambda_b^0) = (5619.7 \pm 1.2\,({\rm stat}) \pm 1.2\,({\rm syst}))\ {\rm MeV}/c^2$. The Λ_b^0 statistical and systematic uncertainties contribute to the systematic uncertainty on the $\Sigma_b^{(*)\pm}$ absolute masses.

Using the measured Q-values we extract the isospin mass splittings for the isotriplets of the $J^P = \frac{1}{2}^+$ and $J^P = \frac{3}{2}^+$ states. The statistical uncertainties on the Q-measurements of the corresponding charge states are added in quadrature. The correlated systematic uncertainties due to mass scale, fit bias due to choice of fit range and imperfect Monte Carlo description of the resolution are largely cancelled in the isospin mass splittings. The uncertainties due to background choice are added in quadrature.

In conclusion, we have measured the masses and widths of the $\Sigma_b^{(*)\pm}$ baryons using a sample of approximately 16 300 Λ_b^0 candidates reconstructed in their $\Lambda_b^0 \to \Lambda_c^+\pi^-$ mode using a sample corresponding to $6\,{\rm fb}^{-1}$ of CDF data.

The first observation [19] of the $\Sigma_b^{(*)\pm}$ bottom baryons has been confirmed with every individual signal reconstructed with a significance well in excess of 6 Gaussian standard deviations.

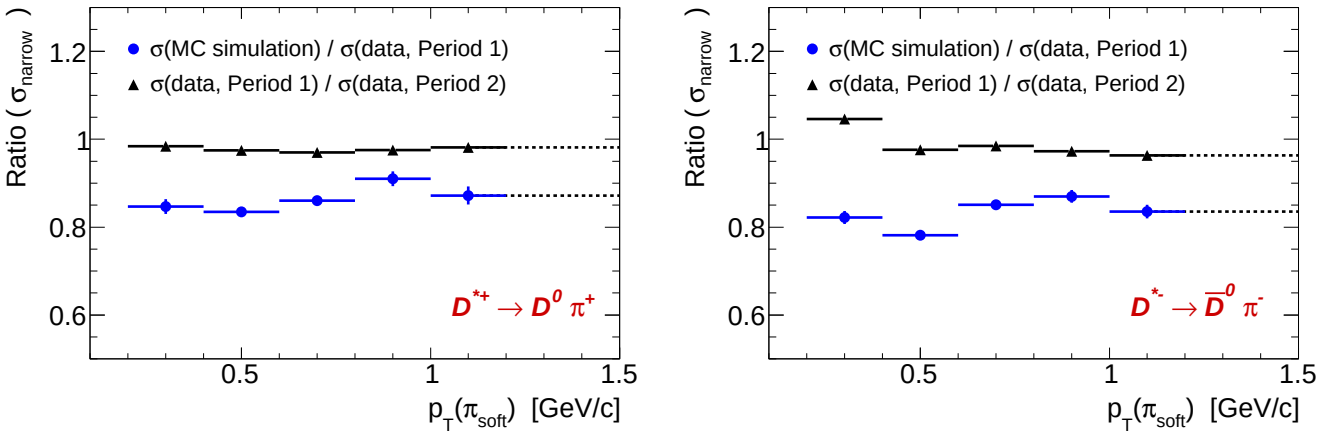

FIG. 4: The left (right) plot shows the ratio of the widths of the narrow component of the D^{*+} (D^{*-}) mass resolution for data and simulation (circles) and for different subsamples of data (triangles) as a function of the transverse momentum of the soft pion.

TABLE V: Summary of the systematic uncertainties. For every measurable quantity, the systematic uncertainties associated with the corresponding sources are listed in the following order: mass scale, fit procedure, resolution, and choice of background model. The total systematic uncertainty is obtained by adding all the associated uncertainties in quadrature. The last column shows, for each measurable quantity, the percentage of the total systematic uncertainty relative to its central value.

Measurable quantity	Scale	Fit	Resolution	Background	Total	Percentage
$Q(\Sigma_b^-)$ [MeV/c^2]		$+0.02$	$+0.06$	$+0.04$	$+0.07$	$+0.1$
	-0.38	-0.03	-0.07	-0.04	-0.39	-0.7
$\Gamma(\Sigma_b^-)$ [MeV/c^2]	$+0.20$	$+0.50$	$+0.85$	$+0.50$	$+1.13$	$+23$
	-0.20	-0.51	-0.87	-0.50	-1.14	-23
$Q(\Sigma_b^{*-})$ [MeV/c^2]		$+0.02$	$+0.06$	$+0.06$	$+0.09$	$+0.1$
	-0.56	-0.09	-0.08	-0.06	-0.58	-0.8
$\Gamma(\Sigma_b^{*-})$ [MeV/c^2]	$+0.20$	$+0.50$	$+0.65$	$+0.30$	$+0.89$	$+12$
	-0.20	-0.90	-0.96	-0.30	-1.36	-18
$Q(\Sigma_b^+)$ [MeV/c^2]		$+0.02$	$+0.07$	$+0.05$	$+0.09$	$+0.2$
	-0.35	-0.03	-0.12	-0.05	-0.38	-0.7
$\Gamma(\Sigma_b^+)$ [MeV/c^2]	$+0.20$	$+0.50$	$+0.94$	$+0.40$	$+1.16$	$+12$
	-0.20	-0.51	-0.90	-0.40	-1.12	-12
$Q(\Sigma_b^{*+})$ [MeV/c^2]		$+0.02$	$+0.06$	$+0.10$	$+0.12$	$+0.2$
	-0.52	-0.09	-0.13	-0.10	-0.55	-0.8
$\Gamma(\Sigma_b^{*+})$ [MeV/c^2]	$+0.20$	$+0.50$	$+0.64$	$+0.50$	$+0.97$	$+8.5$
	-0.20	-0.90	-1.01	-0.50	-1.46	-13

The direct mass difference measurements have a statistical precision that is reduced by a factor of two from previous measurement [19]. The measurements are in good agreement with the previous results and supersede them.

The isospin mass splittings within the $I = 1$ triplets of the Σ_b and Σ_b^* states have been extracted for the first time. The $\Sigma_b^{(*)-}$ states have higher masses than their $\Sigma_b^{(*)+}$ partners, following a pattern common to most of the known isospin multiplets [13]. This measurement favors the phenomenological explanation of this ordering as due to the higher masses of the d quark with respect to the u quark and the larger electromagnetic contribution due to electrostatic Coulomb forces between quarks in $\Sigma_b^{(*)-}$ states than in $\Sigma_b^{(*)+}$ ones. The difference in the measured isospin mass splittings between the Σ_b^* and Σ_b isotriplets supports the theoretical estimate of Ref. [9].

The natural widths of the $\Sigma_b^{\pm}$ and $\Sigma_b^{*\pm}$ states have been measured for the first time. The measurements are in agreement with theoretical expectations.

Acknowledgments

We thank the Fermilab staff and the technical staffs of the participating institutions for their vital contribu-

TABLE VI: Summary of the final results. The first uncertainty is the statistical one and the second is systematic.

State	Q-value, MeV/c^2	Absolute mass m, MeV/c^2	Natural width Γ, MeV/c^2
Σ_b^-	$56.2\,^{+0.6\,+0.1}_{-0.5\,-0.4}$	$5815.5\,^{+0.6}_{-0.5} \pm 1.7$	$4.9\,^{+3.1}_{-2.1} \pm 1.1$
Σ_b^{*-}	$75.8 \pm 0.6\,^{+0.1}_{-0.6}$	$5835.1 \pm 0.6\,^{+1.7}_{-1.8}$	$7.5\,^{+2.2\,+0.9}_{-1.8\,-1.4}$
Σ_b^+	$52.1\,^{+0.9\,+0.1}_{-0.8\,-0.4}$	$5811.3\,^{+0.9}_{-0.8} \pm 1.7$	$9.7\,^{+3.8\,+1.2}_{-2.8\,-1.1}$
Σ_b^{*+}	$72.8 \pm 0.7\,^{+0.1}_{-0.6}$	$5832.1 \pm 0.7\,^{+1.7}_{-1.8}$	$11.5\,^{+2.7\,+1.0}_{-2.2\,-1.5}$
	Isospin Mass Splitting, MeV/c^2		
$m(\Sigma_b^+) - m(\Sigma_b^-)$	$-4.2\,^{+1.1}_{-1.0} \pm 0.1$		
$m(\Sigma_b^{*+}) - m(\Sigma_b^{*-})$	$-3.0\,^{+1.0}_{-0.9} \pm 0.1$		

tions. This work was supported by the U.S. Department of Energy and National Science Foundation; the Italian Istituto Nazionale di Fisica Nucleare; the Ministry of Education, Culture, Sports, Science and Technology of Japan; the Natural Sciences and Engineering Research Council of Canada; the National Science Council of the Republic of China; the Swiss National Science Foundation; the A.P. Sloan Foundation; the Bundesministerium für Bildung und Forschung, Germany; the Korean World Class University Program, the National Research Foundation of Korea; the Science and Technology Facilities Council and the Royal Society, UK; the Russian Foundation for Basic Research; the Ministerio de Ciencia e Innovación, and Programa Consolider-Ingenio 2010, Spain; the Slovak R&D Agency; the Academy of Finland; and the Australian Research Council (ARC).

[1] N. Isgur, M. B. Wise, Phys. Lett. B **232**, 113 (1989); *Ibid.* B **237**, 527 (1990); *Ibid.*, Phys. Rev. D **42**, 2388 (1990).
[2] M. Neubert, Phys. Rept. **245**, 259 (1994);
[3] A. V. Manohar, M. B. Wise, Camb. Monogr. Part. Phys. Nucl. Phys. Cosmol. **10**, 1 (2000).
[4] Throughout the text the notations $\Sigma_b^{(*)}$ or $\Sigma_b^{(*)\pm}$ represent the four states Σ_b^-, Σ_b^{*-}, Σ_b^+ and Σ_b^{*+} while the notations $\Sigma_b^{(*)-}$ or $\Sigma_b^{(*)+}$ include Σ_b^-, Σ_b^{*-} or Σ_b^+, Σ_b^{*+} pairs of states correspondingly.
[5] K. Nakamura *et al.* (Particle Data Group), J. Phys. G **37**, 075021 (2010).
[6] D. Ebert, R. N. Faustov, V. O. Galkin, Phys. Rev. D **72**, 034026 (2005); *Ibid.*, Phys. Lett. B **659**, 612 (2008); *Ibid.*, Phys. Atom. Nucl. **72**, 178 (2009).
[7] E. E. Jenkins, Phys. Rev. D **54**, 4515 (1996); *Ibid.* D **55**, 10 (1997); *Ibid.* D **77**, 034012 (2008).
[8] J. L. Rosner, J. Phys. G **34**, S127 (2007); M. Karliner, H. J. Lipkin, Phys. Lett. B **660**, 539 (2008); M. Karliner, B. Keren-Zur, H. J. Lipkin, J. L. Rosner, arXiv:0708.4027 [hep-ph]; *Ibid.*, Annals Phys. **324**, 2 (2009); M. Karliner, Nucl. Phys. Proc. Suppl. **187**, 21 (2009); H. Garcilazo, J. Vijande, A. Valcarce, J. Phys. G **34**, 961 (2007).
[9] J. L. Rosner, Phys. Rev. D **75**, 013009 (2007).
[10] R. Roncaglia, A. Dzierba, D. B. Lichtenberg, E. Predazzi, Phys. Rev. D **51**, 1248 (1995); R. Roncaglia, D. B. Lichtenberg, E. Predazzi, Phys. Rev. D **52**, 1722 (1995); *Ibid.* D **53**, 6678 (1996).
[11] X. Liu *et al.*, Phys. Rev. D **77**, 014031 (2008); J. R. Zhang, M. Q. Huang, Phys. Rev. D **77**, 094002 (2008).
[12] N. Mathur, R. Lewis, R. M. Woloshyn, Phys. Rev. D **66**, 014502 (2002); R. Lewis, R. M. Woloshyn, Phys. Rev. D **79**, 014502 (2009).
[13] F. K. Guo, C. Hanhart, U. G. Meissner, J. High Energy Phys. 09 (2008) 136.
[14] L. H. Chan, Phys. Rev. D **31**, 204 (1985); W. Y. P. Hwang, D. B. Lichtenberg, Phys. Rev. D **35**, 3526 (1987); S. Capstick, Phys. Rev. D **36**, 2800 (1987); K. Varga, M. Genovese, J. M. Richard, B. Silvestre-Brac, Phys. Rev. D **59**, 014012 (1999); C. W. Hwang, C. H. Chung, Phys. Rev. D **78**, 073013 (2008).
[15] S. Capstick, W. Roberts, Prog. Part. Nucl. Phys. **45**, S241 (2000).
[16] J. G. Korner, M. Kramer, D. Pirjol, Prog. Part. Nucl. Phys. **33**, 787 (1994).
[17] X. H. Guo, K. W. Wei, X. H. Wu, Phys. Rev. D **77**, 036003 (2008).
[18] C. W. Hwang, Eur. Phys. J. C **50**, 793 (2007).
[19] T. Aaltonen *et al.* (CDF Collaboration), Phys. Rev. Lett. **99**, 202001 (2007).
[20] V. M. Abazov *et al.* (DO Collaboration), Phys. Rev. Lett. **99**, 052001 (2007).
[21] T. Aaltonen *et al.* (CDF Collaboration), Phys. Rev. Lett. **99**, 052002 (2007).
[22] T. Aaltonen *et al.* (CDF Collaboration), Phys. Rev. **D80**, 072003 (2009).
[23] V. M. Abazov *et al.* (DO Collaboration), Phys. Rev. Lett. **101**, 232002 (2008).
[24] T. Aaltonen *et al.* (CDF Collaboration), Phys. Rev. Lett. **107**, 102001 (2011).

[25] T. Aaltonen *et al.* (CDF Collaboration), Phys. Rev. **D84**, 012003 (2011).

[26] E. Klempt, J. M. Richard, Rev. Mod. Phys. **82**, 1095 (2010).

[27] D. Acosta *et al.* (CDF Collaboration), Phys. Rev. D **71**, 032001 (2005).

[28] A. Sill *et al.*, Nucl. Instrum. Meth. A **447**, 1 (2000).

[29] A. A. Affolder *et al.* (CDF Collaboration), Nucl. Instrum. Meth. **A453**, 84-88 (2000).

[30] S. Nahn (CDF Collaboration), Nucl. Instrum. Methods A **511**, 20 (2003).

[31] C. S. Hill (On behalf of the CDF Collaboration), Nucl. Instrum. Methods A **530**, 1 (2004).

[32] A. A. Affolder *et al.* (CDF Collaboration), Nucl. Instrum. Methods A **526**, 249 (2004).

[33] E. J. Thomson *et al.*, IEEE Trans. Nucl. Sci. **49**, 1063 (2002).

[34] B. Ashmanskas *et al.* (CDF Collaboration), Nucl. Instrum. Meth. **A518**, 532-536 (2004).

[35] L. Ristori, G. Punzi, Ann. Rev. Nucl. Part. Sci. **60**, 595-614 (2010).

[36] P. Nason, S. Dawson, R. K. Ellis, Nucl. Phys. **B303**, 607 (1988); *Ibid.*, Nucl. Phys. **B327**, 49-92 (1989).

[37] C. Peterson, D. Schlatter, I. Schmitt, P. M. Zerwas, Phys. Rev. **D27**, 105 (1983).

[38] D. J. Lange, Nucl. Instrum. Methods A **462**, 152 (2001).

[39] R. Brun, R. Hagelberg, M. Hansroul, J.C. Lassalle, CERN Reports No. CERN-DD-78-2-REV and No. CERN-DD-78-2.

[40] Unless otherwise stated all references to a specific charge combination imply the charge conjugate combination as well. Specifically, $\overline{\Sigma}_b^{(*)-} \to \overline{\Lambda}_b^0 \pi_s^-$, $\overline{\Sigma}_b^{(*)+} \to \overline{\Lambda}_b^0 \pi_s^+$, $\overline{\Lambda}_b^0 \to \overline{\Lambda}_c^- \pi_b^+$, $\overline{\Lambda}_c^- \to \overline{p} K^+ \pi^-$, $D^{*-} \to \overline{D}^0 (\to K^+ \pi^-) \pi_s^-$.

[41] A. Abulencia *et al.* (CDF Collaboration), Phys. Rev. Lett. **98**, 122002 (2007).

[42] J. D. Jackson, Nuovo Cim. **34**, 1644 (1964).

[43] M. Artuso *et al.* (CLEO Collaboration), Phys. Rev. D **65**, 071101 (2002).

[44] G. Brandenburg *et al.* (CLEO Collaboration), Phys. Rev. Lett. **78**, 2304 (1997).

[45] S.S. Wilks, Ann. Math. Statist. **9** (1938) 60-2.

[46] R. Royall, J. Amer. Statist. Assoc. **95**, 760 (2000).

[47] A. Abulencia *et al.* (CDF Collaboration), Phys. Rev. D **73**, 051104 (2006).

[48] R. Brun, F. Rademakers, Nucl. Instrum. Methods A **389**, 81 (1997); see also `http://root.cern.ch/`.

[49] I. Antcheva *et al.*, Comput. Phys. Commun. **180**, 2499 (2009).

[50] D. E. Acosta *et al.* (CDF Collaboration), Phys. Rev. Lett. **96**, 202001 (2006).